Journal of Power Sources 261 (2014) 1–6

Contents lists available at ScienceDirect

Journal of Power Sources

journal homepage: www.elsevier.com/locate/jpowsour

Novel structure of TiO_2–ZnO core shell rice grain for photoanode of dye-sensitized solar cells

Lixin Song [a,b], Qingxu Jiang [a,b], Pingfan Du [a,b], Yefeng Yang [a,b], Jie Xiong [a,b,*], Can Cui [c]

[a] College of Materials and Textile, Zhejiang Sci-Tech University, Hangzhou 310018, China
[b] Key Laboratory of Advanced Textile Materials and Manufacturing Technology of Ministry of Education, Zhejiang Sci-Tech University, Hangzhou 310018, China
[c] School of Science, Zhejiang Sci-Tech University, Hangzhou 310018, China

HIGHLIGHTS

- TiO_2–ZnO core shell rice grains were prepared via coaxial electrospinning.
- The core shell rice grains are as the photoanodic material of DSSC.
- The potential application of the method and nanostructures are suggested.

GRAPHICAL ABSTRACT

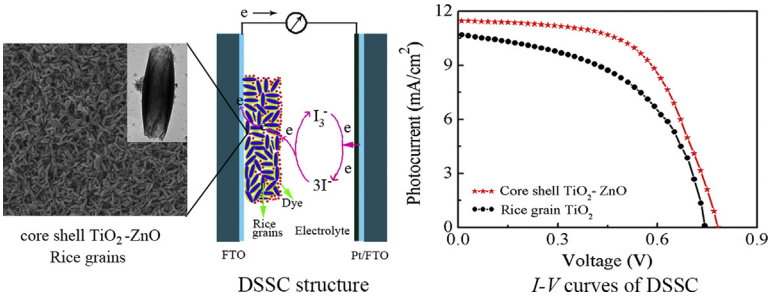

ARTICLE INFO

Article history:
Received 12 November 2013
Received in revised form
23 January 2014
Accepted 12 March 2014
Available online 19 March 2014

Keywords:
Titanium dioxide
Zinc oxide
Core shell
Rice grain
Dye-sensitized solar cells

ABSTRACT

The TiO_2–ZnO core shell rice grains are prepared by coaxial electrospinning and calcination. These core shell rice grains have the length of 300–800 nm and the BET surface area of 66.3 $m^2\ g^{-1}$. They consist of anatase TiO_2 (core) and wurtzite ZnO (shell). Using this novel structure as the photoanodic material, the dye-sensitized solar cells (DSSCs) have the conversion efficiency (η) of 5.31%, which is increased by 23.9% in comparison with that of the DSSCs based on the TiO_2 rice grains. This is mainly ascribed to the improvement in both light harvesting efficiency and electron collection efficiency, and the effective suppression of charge recombination.

1. Introduction

Dye-sensitized solar cells (DSSCs) have attracted great interest as one of the most potential photovoltaic devices owing to their low cost and easy fabrication [1–3]. However, the conversion efficiency of most DSSCs is still a bit low despite the highest record has reached 12.3% [4]. Further improvement in conversion efficiency is necessary for DSSCs. To date, diverse efforts on optimizing and modifying TiO_2 nanocrystalline film have intensively taken to improve the conversion efficiency of DSSCs [5–7].

One effective way to improve the properties of DSSCs is that one dimensional (1D) nanostructures such as nanowires (NWs), nanotubes (NTs), and nanofibers (NFs) replace of zero-dimensional (0D) nanoparticles (NPs). The 1D nanostructure can be beneficial to

* Corresponding author. Key Laboratory of Advanced Textile Materials and Manufacturing Technology of Ministry of Education, Zhejiang Sci-Tech University, Hangzhou 310018, China. Tel.: +86 751 86843603.
E-mail address: jxiong@zstu.edu.cn (J. Xiong).

http://dx.doi.org/10.1016/j.jpowsour.2014.03.030
0378-7753/

electron transport due to less grain boundaries, less surface states (i.e., recombination sites), and direct pathways for charges in comparison of NPs [8–11]. As a simple, low-cost, and easy scale technique, electrospinning is employed to fabricate 1D nanostructure (NFs, NRs, and NWs) for DSSCs by some groups [12–15]. Recently, Ramakrishna et al. reported that a novel structure (rice grain) TiO_2 fabricated by electrospinning acted as photoanode material and enhanced the conversion efficiency of DSSCs owing to its more excellent inter-grain connectivity and higher surface area than P25 [16,17]. Subsequently, they found that the rice grain shaped TiO_2 exhibited the better scattering effect to increase the capability of photoanode to harvest light than TiO_2 NFs [18] and the CNT doping in rice grain shaped TiO_2 can further improve the conversion efficiency [19].

As we all known, a core shell structure that TiO_2 are coated by another higher conduction band metal oxide semiconductor (ZnO, Nb_2O_5, Al_2O_3, MgO, etc.) forms an energy barrier to facilitate the charge separation and to reduce the electron recombination [20–22]. Among the numerous semiconductors oxide, ZnO is an excellent coating material to modify TiO_2 due to their similar energy band structure [23], higher electron mobility [24], and a lower photo inactivation [25] in comparison of TiO_2. Although the TiO_2–ZnO core shell nanostructures such as NPs [26], NWs [27], and NFs [28] for DSSCs can enhance the conversion efficiencies compared with the TiO_2 nanostructures, the efficiencies is still a bit low (a highest efficiency of 5.17% for nanofibers). If the TiO_2 rice grain could be coated by other metal oxide semiconductor to form a core shell structure, this novel structure as photoanodic material may further enhance the conversion efficiency of DSSCs. Up to now, no paper concerning core shell rice grain based DSSCs has been reported.

Based on the above, in this work, the TiO_2–ZnO core shell rice grains are fabricated by coaxial electrospinning and calcination. The photovoltaic performance of DSSCs employing the core shell rice grains were investigated in detail.

2. Experimental details

2.1. Preparation of TiO_2–ZnO core shell rice grains

The TiO_2–ZnO core shell rice grains were synthesized by coaxial electrospinning and calcination according to the following route: 0.61 g of polyvinyl acetate (PVAc, M_w = 500,000, Aldrich) was dissolved in 5 mL of *N*,*N*-dimethyl acetamide (DMAc, 99.5%, Aladdin). Then, 1 mL of acetic acid and 0.5 mL titanium (IV) isopropoxide (TiP, Aldrich) were added in the above solution to form TiO_2 precursor electrospinning solution A; meanwhile, 0.96 g of PVAc and 0.64 g of zinc acetate dihydrate [$Zn(CH_3COO)_2{\cdot}2H_2O$, 99%, Aladdin] was dissolved in 8 mL of *N*,*N*-dimethyl formamide (DMF, 99.5%, Aladdin) to obtain ZnO precursor electrospinning solution B. The solutions A and B were transferred into two different glass syringes. The precursor solutions were electrospun on the collector via coaxial electrospinning with the core flow rate of 0.5 mL h^{-1} for solution A, the shell flow rate of 0.6 mL h^{-1} for the solution B, and a voltage of 20 kV. The collector was kept 10 cm away from the nozzle tip (RH 50–60%, 20–25 °C). For comparison, the solution A was electrospun to get TiO_2 rice grains. Finally, both the as-spun samples were calcined in a muffle furnace at 500 °C for 1 h.

2.2. Assembling DSSCs

The photoanodic film was fabricated via spin coating. In a typical process, 100 mg of the TiO_2–ZnO core shell rice grains mixed with 200 mg of polyethylene glycol (PEG, M_w = 20,000, Aladdin) were added in 1.5 mL deionized water. Then the mixture was stirred for 4 h to obtain a unique paste of right rheology necessary for spin coating. The paste was spin coated to get an overall thickness of ~12 μm on the clean fluorine-doped tin oxide (FTO, 15 Ω sq^{-1}) plate. The paste along with FTO was calcined in air at 500 °C for 30 min to get porous film with the thickness of ~8 μm (This is due to the evaporation of the organics from the mixture during calcination) and the active area of 0.36 cm^2. For comparison, the rice grain shaped TiO_2 photoanodic film was prepared by the same process as the above film. Subsequently the two films along with FTO were soaked in 0.5 mM N719 dye solution (in 1:1 acetonitrile and tert-butanol mixture) for 24 h. The photoanodes were washed with absolute ethanol for removing the unanchored dyes. The photoanodes were sandwiched against the Pt counter-electrodes in the presence of 60 μm sealing spacer (Surlyn 1702, DuPont) and I_3^-/I^- electrolyte to assemble DSSCs.

2.3. Characterization

The X-ray diffraction (XRD) patterns of the samples were conducted on a Thermo ARL-X'TRA using a Ni-filtered Cu Kα radiation (λ = 1.5418 Å), and scans were made from 15° to 75° (2θ) at the speed of 2° min^{-1}. The morphologies of the samples were conducted by the field emission scanning electron microscope (FESEM, ULTRA 55, ZEISS, Germany) and transmission electron microscope (TEM, JEM2100, Japan). The Brunauer–Emmett–Teller (BET) of the samples was measured by a surface area and porosity analyzer (Micromeritics ASAP 2020 Accelerated Surface Area and Porosimetry System, USA) using N_2 adsorption at 77 K. The amount of loading dye molecules was determined by detaching dye from the photoanode into 1.0 M NaOH aqueous solution and measuring the absorption spectra of N719 solution on a UV–vis spectrophotometer (Lambda 900, Perkin Elmer). The photocurrent–voltage (*I*–*V*) characteristic was performed with a sourcemeter (2400-SCS, Keithley) under 100 mW cm^{-2} illumination. The solar simulator consists of a 500 W Xe lamp (Trusttech, China) and an AM 1.5 filter (Oriel). A QE/IPCE test system (Solar Cell Scan100/Zolix) was used to measure the incident photo-to-electron conversion efficiency (IPCE) of DSSCs. The electrochemical impedance spectroscopy (EIS) measurements were measured in the dark using a potentiostat (Im6ex/Zahner) under 0.7 V forward bias and 10 mV AC amplitude, and the frequency range was 0.01–100 kHz.

3. Results and discussion

3.1. The morphology and structures of the samples

Fig. 1 exhibits the XRD patterns of the as-spun PVAc/TiP–PVAc/$Zn(CH_3COO)_2$ composite NFs, and the two kinds of composite NFs

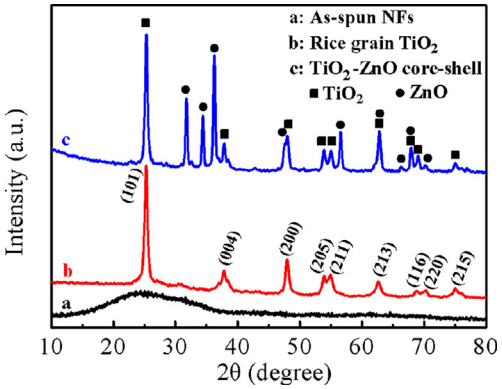

Fig. 1. XRD patterns of the as-spun PVAc/TiP–PVAc/$Zn(CH_3COO)_2$ NFs, the rice grain shaped TiO_2, and the rice grain shaped TiO_2–ZnO core shell structures.

[PVAc/TiP and PVAc/TiP–PVAc/$Zn(CH_3COO)_2$] after calcination. The as-spun composite NFs are in an amorphous phase as shown in Fig. 1a. The PVAc/TiP NFs after calcination can be indexed to anatase TiO_2 according to the standard JCPDS card (No. 21-1272) as depicted in Fig. 1b. After the composite PVAc/TiP–PVAc/$Zn(CH_3COO)_2$ NFs were calcined in Fig. 1c, the anatase TiO_2 and wurtzite ZnO (JCPDS card No. 36-1451) are observed with no additional peaks for other phases. The sharp shapes and line widths of these diffraction peaks indicate that both TiO_2 and ZnO have excellent crystallization.

The FESEM, TEM, and HRTEM images of the PVAc/TiP–PVAc/$Zn(CH_3COO)_2$ NFs before and after calcination are shown in Fig. 2. From Fig. 2a, it can be seen that these as-spun NFs are randomly oriented and have smooth surfaces. All the NFs are consisting of alternating nubs and shafts. The length of the nub in NFs is 1 ± 0.3 μm. The as-spun NF consists of a nearly axisymmetric core sheath structure and the thickness of the shell is dozens of nanometers as depicted in Fig. 2c. Interestingly, after calcination in Fig. 2b, the fiber structure has disappeared and the nubs change into rice grains with the length of 300–800 nm. The desired core shell structure is still maintained in the rice grain as exhibited in Fig. 2d. The lattice resolved images of the TiO_2–ZnO core shell rice grains are displayed in Fig. 2e and f. The lattice spacing of 0.35 nm (on the end of the rice grain) corresponds to the (101) plane of anatase TiO_2, and the lattice spacing of the surface of core shell rice grains (Fig. 2d) is 0.52 nm due to the (001) plane of ZnO in Fig. 2f.

To further characterize the rice grains, the XPS measurements were conducted. In the XPS full spectra of bare TiO_2 as shown in Fig. 3a, two main peaks with binding energies of 453.5 and 526.8 eV are respectively attributed to Ti 2p3/2 and O1s [29,30]. For the core–shell structure [Fig. 3a], two strong additional peaks with the binding energy of 1043.2 eV and 1021.5 eV respectively correspond to Zn 2p1 and Zn 2p3. The O 1s XPS spectra for the two samples are depicted in Fig. 3b. The O 1s peak of TiO_2 locates at about 529.4 eV. Accompanied by a significant decline in the intension of O 1s peak of TiO_2, a strong peak of O 1s with the bonding energy of 529.8 eV appears. The peak is attributed to the ZnO in TiO_2–ZnO core shell rice grains [30]. In Fig. 3c, a careful comparison of the Ti 2p region of TiO_2 and TiO_2/ZnO exhibit that two peaks located at about 457 and 464 eV, which are assigned to Ti 2p3/2 and Ti 2p1/2, respectively. It can be seen that the binding energy of Ti 2p3/2 for the TiO_2 (456.8 eV), implying the formation of the Ti^{4+} and Ti^{3+} species on the surface of TiO_2 [31,32]. While, a slight deformation in the higher side of the binding energy of Ti 2p3/2 exhibited in TiO_2/ZnO. The TiO_2 coated by ZnO reduced the amounts of Ti^{3+} that can serve as

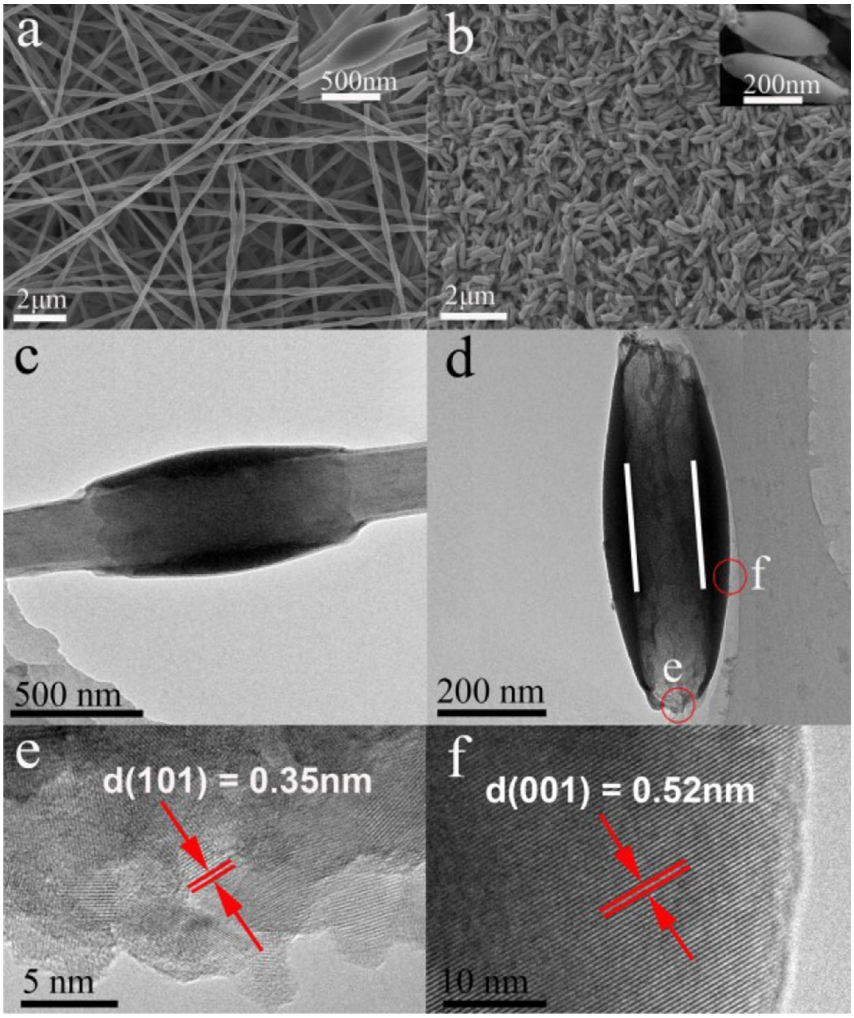

Fig. 2. FESEM (a and b), TEM (c and d) of the fibers before and after calcination, and HRTEM (e and f) of TiO_2–ZnO core shell rice grain.

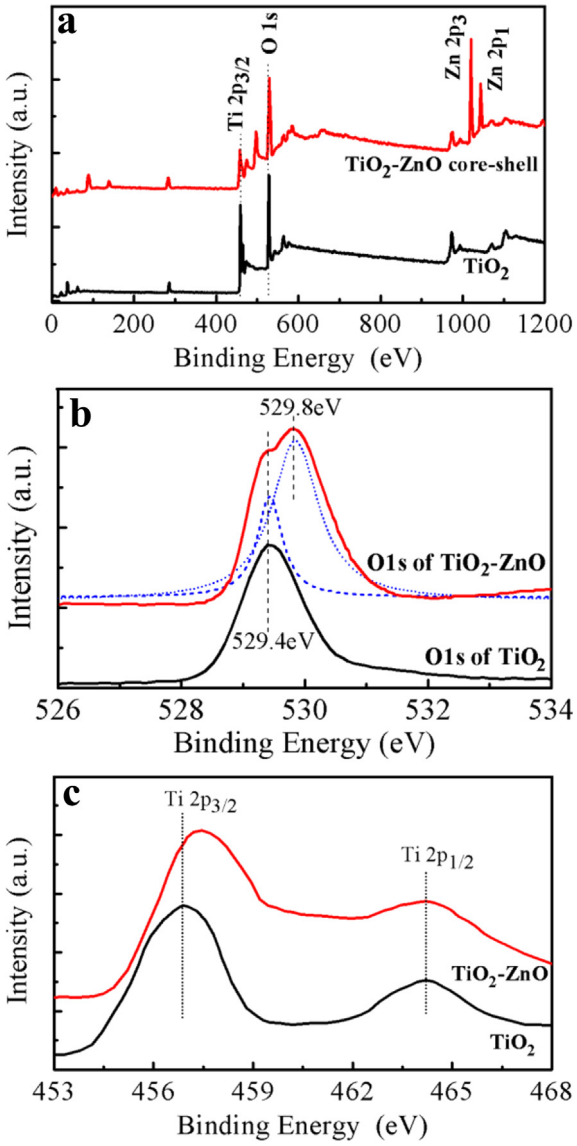

Fig. 3. XPS spectrum of rice grain shaped TiO_2 and rice grain shaped TiO_2–ZnO core–shell: (a) the full spectra, (b) the O 1s narrow range scan spectra, and (c) the Ti 2p narrow range scan spectra.

recombination centers and pathways for electron back transfer [33,34].

The results of XRD, TEM, and XPS absolutely confirm that the TiO_2–ZnO core shell structures form (The TiO_2 is shielded by an external ZnO shell despite a few regions (both the ends) at the surface of TiO_2 rice grains are not coated totally by ZnO). Therefore, the formation of rice grains could be attributed to as follows: In as-spun composite NFs, the precursors of TiO_2 and ZnO are mainly concentrated in the nubs (Each nub contains a little of PVAc) due to the phase separation between the precursor and PVAc. The shafts in NFs mainly consist of PVAc. During calcination, the decomposition of PVAc in shafts broke the NFs. Meanwhile, the core shell nubs grow into the rice grain shaped structures through the decomposition of the precursors and PVAc, and the growth of ZnO and TiO_2. In other words, the as-spun core shell nubs act the structure directing template for the formation of the core shell rice grains. Moreover, the sizes of the rice grains are smaller than the nubs due to the decomposition of the precursors and PVAc.

3.2. The photovoltaic properties of the DSSCs

Fig. 4 depicts the *I–V* characteristics of the DSSCs based on TiO_2 rice grains and TiO_2–ZnO core shell rice grains. As shown in Table 1, all the photovoltaic parameters of TiO_2–ZnO core shell rice grains based DSSCs were higher than those of the DSSCs based on TiO_2 rice grains. The conversion efficiency (η) increased from 4.14% to 5.31% due to the increasing of the open circuit voltage (V_{oc}), the current density (J_{sc}), and the fill factor (FF) with the addition of ZnO layer. Moreover, the improvement in conversion efficiency is further reflected in the IPCE (as a function of wavelength) of the two DSSCs. In Fig. 4b, the IPCE of the DSSCs using TiO_2–ZnO core shell rice grains are higher than those of DSSCs fabricated by TiO_2 rice grains in all the wavelengths.

Generally, the IPCE and J_{sc} are related to the light harvesting [LHE(λ)], charge injection (Φ_{inj}), and charge collection (Φ_c) according to Equation (1) [35,36] and Equation (2) [37,38], respectively.

$$\mathrm{IPCE}(\lambda) = \mathrm{LHE}(\lambda)\Phi_{\mathrm{inj}}\Phi_{\mathrm{c}} \tag{1}$$

$$J_{\mathrm{sc}} = \int e\mathrm{IPCE}(\lambda)I_{\mathrm{S}}(\lambda)d\lambda \tag{2}$$

The LHE(λ) is a strong function of the dye-loading. The dye-loading of the TiO_2–ZnO core shell rice grain photoanodic film was higher than that of TiO_2 rice grain electrodes as exhibited in Fig. 5a, which is attributed to their BET surface areas (The BET surface area of TiO_2 rice grains and TiO_2–ZnO core shell rice grains are about 58.5 $m^2\ g^{-1}$ and 66.3 $m^2\ g^{-1}$, respectively). Φ_{inj} is related to energetic discrepancy between the excited level of the dye (E_{ex}) and the conduction band edge (E_{cb}) of the photoanode oxide. The E_{cb} of ZnO is a bit positive than that of TiO_2 resulting in the energetic discrepancy decreasing slightly, but the biased energy band structure enhances the separation efficiency of charges leading to the increased Φ_{inj} (Fig. 5b) [27]. Thus, the Φ_{inj} have a trivial effect on the IPCE and J_{sc}. Φ_c depends on electron transport and charge recombination in DSSCs. Fig. 6a and b exhibits the schematic diagram of the electron transport in DSSCs based on TiO_2–ZnO core shell rice grains. In Fig. 6a, the rice grains provide the directly pathways for the electron from the dye to FTO glass to accelerate the charges flow [17]. Besides, the injected electron can be enhanced resulting from the steps with two energy level facilitating the charge separation [39] and the energy barrier reducing the charges recombination as displayed in Fig. 6b [5]. The electrons transport and charges recombination in DSSCs can be characterized

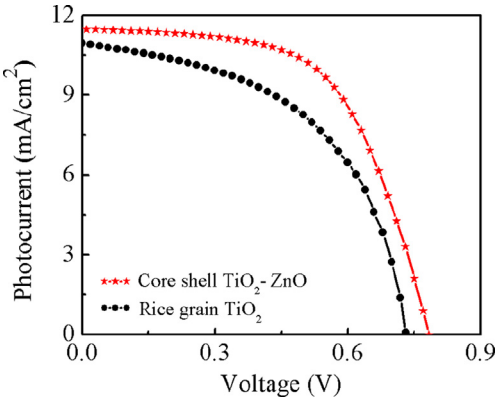

Fig. 4. *I–V* curves of DSSCs based on TiO_2 rice grains and TiO_2–ZnO core shell rice grains.

Table 1
The photovoltaic properties of DSSCs using TiO_2 rice grains and TiO_2–ZnO core shell rice grains.

DSSCs	V_{oc}/V	J_{sc}/mA cm^{-2}	FF/%	η/%
Rice grain TiO_2	0.732	10.9	51.9	4.14
TiO_2–ZnO core shell	0.783	11.5	59.0	5.31

by the EIS (electrochemical impedance spectrum). Fig. 6c shows EIS spectra of the two DSSCs (in the dark). The Nyquist plots of the two cells are in a shape of a large semicircle due to the other two semicircles being overshadowed by the large one [40,41]. In general, the semicircle on the Nyquist plot in this frequency range is associated with the charge transfer across the photoanode/electrolyte interface, and the recombination rate between electrons in the photoanode and holes in the electrolyte is inversely proportional to the size of this semicircle [42,43]. It is obvious that the semicircle in TiO_2–ZnO core shell based DSSC is larger than that of TiO_2 rice grain based DSSC as displayed in Fig. 6c. In the dark, the larger the size of this semicircle, the lower the charge recombination rate could be [28,44]. Consequently, the Φ_c of DSSCs employing TiO_2–ZnO core shell is the larger than that of the DSSCs based on TiO_2 rice grains.

The V_{oc} depends on the different values between the Fermi level of photoanode oxide and redox potential of I^-/I_3^-. The higher V_{oc} results from the slight E_{cb} positive shift of the photoanode with addition of ZnO layer. Besides, the increase in V_{oc} can be well understood according to the following equation [45,46]:

$$V_{oc} = \left(kT/e\right)\ln\left(I_{inj}/(n_{cb}K_rK_c)\right) \quad (3)$$

where I_{inj} is the incident photon flux, n_{cb} is the electron density in the photoanodic film, K_r is the rate constant for the back electron transfer, K_c is the concentration of triiodide species in electrolyte. The K_r in DSSCs decreased with addition of ZnO coating due to reducing the recombination as shown in Fig. 6c. Thus, the increased I_{inj} and the decreased K_r lead to the increase of V_{oc}. The improvement in FF may also contribute to that the ZnO layer inhibits electron back transfer from TiO_2 to the redox electrolyte [18]. The simultaneous increases of J_{sc}, V_{oc}, and FF result in the improvement of the conversion efficiency.

4. Conclusions

The rice grain shaped TiO_2–ZnO core shell structures have been successfully prepared via a combined method of coaxial electro spinning and calcination. The TiO_2–ZnO core shell rice grains have the length of about 300–800 nm and consist of anatase TiO_2 (core) and wurtzite ZnO (shell). With the DSSC fabricated by TiO_2–ZnO core shell rice grains, its conversion efficiency is 5.31%, which exhibits improvements of 23.9% over the DSSC based on TiO_2 rice grains. This improvement in conversion efficiency is mainly due to the increase of the loading dye, the charge recombination being suppressed by the energy barrier of ZnO layer, and the increased separation efficiency of charges by the biased energy band structure. This work provides useful insights for the development of novel nanoscale photoanodic structures of DSSCs. And the TiO_2–ZnO core shell rice grains can be applied in photocatalysis.

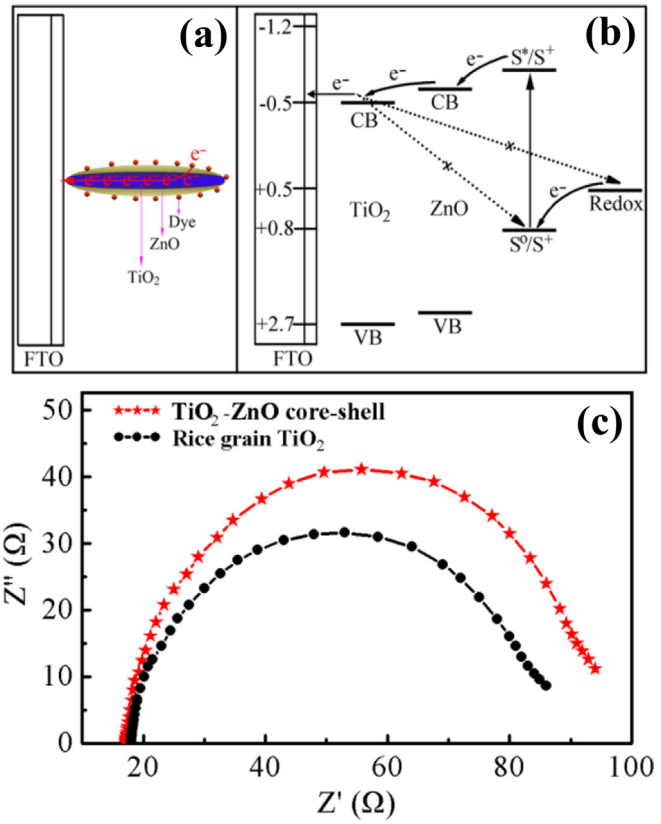

Fig. 6. Schematic diagram of two effects arising from ZnO–TiO_2 core shell rice grain: the direct pathways for charges (a), and TiO_2–ZnO heterojunction forms biased energy band structure to enhance electron separation efficiency and ZnO shell introduces an interfacial energy barrier to suppress recombination (b); and EIS of TiO_2 rice grains and TiO_2–ZnO core shell based DSSCs in the dark (c).

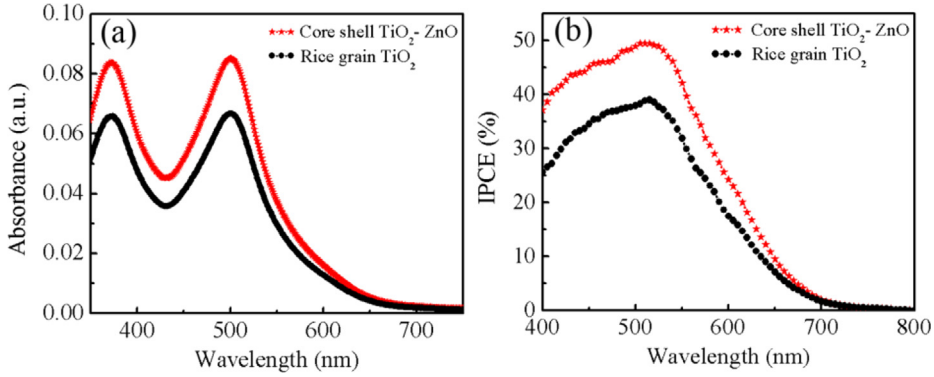

Fig. 5. UV–vis absorption spectra of solutions containing N719 dye detached from TiO_2 rice grain and TiO_2–ZnO core shell rice grain electrodes (a), and IPCE spectra of DSSCs based on the two electrodes (b).

Acknowledgment

The financial support of this work was provided by Top Priority Discipline of Textile Science and Engineering of Zhejiang Province for Cultivation of Outstanding Graduate Thesis (2013YBPY06), Special Program for International S&T Cooperation Projects of Zhejiang Province (2012C24012), and Program for Zhejiang Leading Team of Science and Technology Innovation (2011R50003).

References

[1] B. O'Regan, M. Grätzel, Nature 353 (1991) 737–740.
[2] B. Liu, E.S. Aydil, J. Am. Chem. Soc. 131 (2009) 3985–3990.
[3] Y.Y. Zhang, J. Khamwannah, H. Kim, S.Y. Noh, H.B. Yang, S.H. Jin, Nanotechnology 24 (2013) 045401.
[4] A. Yella, H.W. Lee, H.N. Tsao, C. Yi, A.K. Chandiran, M.K. Nazeeruddin, E.W.G. Diau, C.Y. Yeh, S.M. Zakeeruddin, M. Grätzel, Science 334 (2011) 629–633.
[5] Q. Hu, C.C. Wu, L.Q. Cao, B. Chi, J. Pu, L. Jian, J. Power Sources 226 (2013) 8–15.
[6] L.J. Yang, W.W.F. Leung, Adv. Mater. 25 (2013) 1792–1795.
[7] P.Y. Chen, X.N. Dang, M.T. Klug, J. Qi, N.M.D. Courchesne, F.J. Burpo, N. Fang, P.T. Hammond, A.M. Belcher, ACS Nano 7 (2013) 6563–6574.
[8] J.Z. Chen, B. Li, J.F. Zheng, S.P. Jia, J.H. Zhao, H.W. Jing, Z.P. Zhu, J. Phys. Chem. C 115 (2011) 7104–7113.
[9] H. Yu, S.Q. Zhang, H.J. Zhao, B.F. Xue, P.R. Liu, G. Will, J. Phys. Chem. C 113 (2009) 16277–16282.
[10] G.K. Mor, K. Shankar, M. Paulose, O.K. Varghese, C.A. Grimes, Nano Lett. 6 (2006) 215–218.
[11] M. Adachi, Y. Murata, J. Takao, J.T. Jiu, M. Sakamoto, F.M. Wang, J. Am. Chem. Soc. 126 (2004) 14943–14949.
[12] M.Y. Song, D.K. Kim, K.J. Ihn, S.M. Jo, D.Y. Kim, Nanotechnology 15 (2004) 1861–1865.
[13] K. Onozuka, B. Ding, Y. Tsuge, T. Naka, M. Yamazaki, S. Sugi, S. Ohno, M. Yoshikawa, S. Shiratori, Nanotechnology 17 (2006) 1026–1031.
[14] K. Fujihara, A. Kumar, R. Jose, S. Ramakrishna, S. Uchida, Nanotechnology 18 (2007) 365709.
[15] X. Zhang, V. Thavasi, S.G. Mhaisalkar, S. Ramakrishna, Nanoscale 4 (2012) 1707–1716.
[16] A.S. Nair, S.Y. Yang, P.N. Zhu, S. Ramakrishna, Chem. Commun. 46 (2010) 7421–7423.
[17] S.Y. Yang, P.N. Zhu, A.S. Nair, S. Ramakrishna, J. Mater. Chem. 21 (2011) 6541–6548.
[18] P.N. Zhu, A.S. Nair, S.Y. Yang, S.J. Peng, S. Ramakrishna, J. Mater. Chem. 21 (2011) 12210–12212.
[19] P.N. Zhu, A.S. Nair, S.Y. Yang, S.J. Peng, N.K. Elumalai, S. Ramakrishna, J. Photochem. Photobiol. A 231 (2012) 9–18.
[20] V. Ganapathy, B. Karunagaran, S.W. Rhee, J. Power Sources 195 (2010) 5138–5143.
[21] D.B. Menzies, Q. Dai, L. Bourgeois, R.A. Caruso, Y.B. Cheng, G.P. Simon, L. Spiccia, Nanotechnology 18 (2007) 125608.
[22] Y. Diamant, S. Chappel, S.G. Chen, O. Melamed, A. Zaban, Coord. Chem. Rev. 248 (2004) 1271–1276.
[23] S. Sakthivel, B. Neppolian, M.V. Shankar, B. Arabindoo, M. Palanichamy, V. Murugesan, Sol. Energy Mater. Sol. Cells 77 (2003) 65–82.
[24] A.B.F. Martinson, M.S. Goes, F.F. Santiago, J. Bisquert, M.J. Pellin, J.T. Hupp, J. Phys. Chem. A 113 (2009) 4015–4021.
[25] R.J. Barnes, R. Molina, J.B. Xu, P.J. Dobson, I.P. Thompson, J. Nanopart. Res. 15 (2013) 1432.
[26] K. Park, Q.F. Zhang, B.B. Garcia, G.Z. Cao, J. Phys. Chem. C 115 (2011) 4927–4934.
[27] Y.L. Xie, Z.X. Li, Z.G. Xu, H.L. Zhang, Electrochem. Commun. 13 (2011) 788–791.
[28] P.F. Du, L.X. Song, J. Xiong, N. Li, Z.Q. Xi, L.C. Wang, D.L. Jin, S.Y. Guo, Y.F. Yuan, Electrochim. Acta 78 (2012) 392–397.
[29] X.T. Zhang, I. Sutanto, T. Taguchi, K. Tokuhiro, Q.B. Meng, T.N. Rao, A. Fujishima, H. Watanabe, T. Nakamori, M. Uragami, Sol. Energy Mater. Sol. Cells 80 (2003) 315–326.
[30] S.H. Kang, J.Y. Kim, Y. Kim, H.S. Kim, Y.E. Sung, J. Phys. Chem. C 111 (2007) 9614–9623.
[31] K.H. Park, M. Dhayal, Electrochem. Commun. 11 (2009) 75–79.
[32] G.X. Cao, Y.G. Li, Q.H. Zhang, H.Z. Wang, J. Hazard. Mater. 178 (2010) 440–449.
[33] X.B. Zhang, H.M. Tian, X.Y. Wang, G.G. Xue, Z.P. Tian, J.Y. Zhang, S.K. Yuan, T. Yu, Z.G. Zou, Mater. Lett. 100 (2013) 51–53.
[34] Y. Yu, K.J. Wu, D.L. Wang, Appl. Phys. Lett. 99 (2011) 192104.
[35] M. Grätzel, Inorg. Chem. 44 (2005) 6841–6851.
[36] Q.F. Zhang, C.S. Dandeneau, X.Y. Zhou, G.Z. Cao, Adv. Mater. 21 (2009) 4087–4108.
[37] M. Grätzel, Acc. Chem. Res. 42 (2009) 1788–1798.
[38] Y.P. Lin, S.Y. Lin, Y.C. Lee, Y.W.C. Yang, J. Mater. Chem. A 1 (2013) 9875–9884.
[39] J.S. Im, J. Yun, S.K. Lee, Y.S. Lee, J. Alloys Compd. 513 (2012) 573–579.
[40] A.S. Nair, R. Jose, S.Y. Yang, S. Ramakrishna, J. Colloid Interface Sci. 353 (2011) 39–45.
[41] M.Y. Song, D.K. Kim, K.J. Ihn, S.M. Jo, D.Y. Kim, Synth. Met. 153 (2005) 77–80.
[42] C.K. Xu, J.M. Wu, U.V. Desai, D. Gao, Nano Lett. 12 (2012) 2420–2424.
[43] Q. Wang, J.E. Moser, M. Grätzel, J. Phys. Chem. B 109 (2005) 14945–14953.
[44] K.M. Lee, V. Suryanarayanan, K.C. Ho, J. Power Sources 188 (2009) 635–641.
[45] D. Hwang, S.M. Jo, D.Y. Kim, V. Armel, D.R. MacFarlane, S.Y. Jang, ACS Appl. Mater. Interfaces 3 (2011) 1521–1527.
[46] Z.S. Wang, C.H. Huang, Y.Y. Huang, Y.J. Hou, P.H. Xie, B.W. Zhang, H.M. Cheng, Chem. Mater. 13 (2001) 678–682.